Available online at www.sciencedirect.com
ScienceDirect
Journal of Sound and Vibration 318 (2008) 166–175
JOURNAL OF SOUND AND VIBRATION
www.elsevier.com/locate/jsvi

Instability analysis in oscillators with velocity-modulated time-varying stiffness—Applications to gears submitted to engine speed fluctuations

G. Sika, Ph. Velex*

LaMCoS, UMR CNRS 5219, INSA Lyon, France

Received 23 March 2007; received in revised form 14 January 2008; accepted 7 April 2008
Handling Editor: M.P. Cartmell
Available online 21 May 2008

Abstract

A one degree-of-freedom model is set up which incorporates time-varying mesh stiffness functions and the influence of unsteady input rotations due to engine speed fluctuations. The stability of the associated parametrically excited system is analysed by calculating the monodromy matrix via a Newmark scheme. A piecewise constant and a sinusoidal mesh stiffness functions are considered and it is shown that additional side-band instability zones are generated because of frequency modulations. The influence of the mesh stiffness variations and damping is discussed.

1. Introduction

In this paper, the contribution of velocity-modulated time-varying stiffness functions on dynamic stability is investigated. The practical application concerns geared systems submitted to velocity fluctuations generated by live reciprocating engine combustion and inertial effects [1]. As far as the authors are aware, the influence of this phenomenon on gear dynamic stability has received very little attention and most of the papers in the literature deal mainly with the analysis of amplitude jumps and rattle noise when contacts between the teeth are temporarily lost [2,3]. The stability analyses are conducted based on a differential equation with frequency-modulated multi-harmonic parametric excitations and stability charts are derived which, in the particular case of gears, illustrate the role of some design parameters.

2. Model

The following assumptions have been considered: (i) tooth shapes are perfect involutes with neither profile nor lead modifications, (ii) the pinion speed $\Omega_1(t)$ for rigid-body conditions and the output torque C_R are imposed (known), and (iii) friction torques are neglected compared to those generated by the

*Corresponding author. Tel.: +33 4 72 43 84 51; fax: +33 4 78 89 09 80.
E-mail address: Philippe.Velex@insa-lyon.fr (P. Velex).

0022-460X/$ - see front matter
doi:10.1016/j.jsv.2008.04.008

Nomenclature

C_M, C_R torque on pinion, on gear
I_1, I_2 pinion, gear polar moment of inertia
R_{b1}, R_{b2} pinion, gear base radii
$u = ((-R_{b1})/R_{b2})$ speed ratio
Z_1, Z_2 tooth number on pinion, on gear

Greek symbols

α relative amplitude variation of mesh stiffness
β_b base helix angle
Δ mesh deflection
ε damping factor
ρ_k dimensionless amplitude of speed fluctuation (harmonic k)
$\vartheta = \int_0^t \Omega_1(\xi)\,\mathrm{d}\xi$ time-dependent pinion angular variable
θ_1, θ_2 torsional degrees of freedom on pinion, on gear
ω_0 natural frequency of the system with averaged mesh stiffness
Ω_{10} average (nominal) rigid-body angular velocity of pinion
$\Omega_1(t), \Omega_2(t) = u\Omega_1(t)$ rigid-body angular velocity of pinion, of gear

normal forces on the mating flanks. The mechanical model shown in Fig. 1 stems from the classic one degree-of-freedom system which has been widely used for the simulation of gear nonlinear dynamic behaviour since the late 1950s [4–7]. Introducing the mesh deflection $\Delta = \cos\beta_b(R_{b1}\theta_1 + R_{b2}\theta_2)$, the semi-definite equations of motion are transformed into the following differential equation (see Nomenclature):

$$\ddot{\Delta} + 2\varepsilon\omega_0\dot{\Delta} + \omega_0^2(1 + \alpha\phi(t))\Delta = \Gamma(t), \tag{1}$$

where ε is the damping factor; $\omega_0 = \cos\beta_b\sqrt{k_m/\bar{M}}$ is the natural frequency associated with the averaged mesh stiffness k_m; $\bar{M} = I_1I_2/(I_1R_{b2}^2 + I_2R_{b1}^2)$ is the equivalent mass; $\Gamma(t) = (\cos\beta_b/\bar{M}R_{b2})(C_R + uI_2\dot{\Omega}_1(t))$ represents the sum of the nominal resisting torque along with the inertial torque caused by acceleration; $\phi(t)$ accounts for the time variations of the mesh stiffness function; θ_1, θ_2 are the small torsional angles superimposed on rigid-body rotations for the pinion and the gear.

Depending on engine technology, ignition order, etc., pinion angular velocity and torque fluctuate periodically as shown in Fig. 2. A general expression of the pinion speed for rigid-body conditions is introduced via a Fourier series as:

$$\Omega_1(t) = \Omega_{10}\left[1 + \sum_k \rho_k \sin(k\Omega_{10}t + \varphi_k)\right], \tag{2}$$

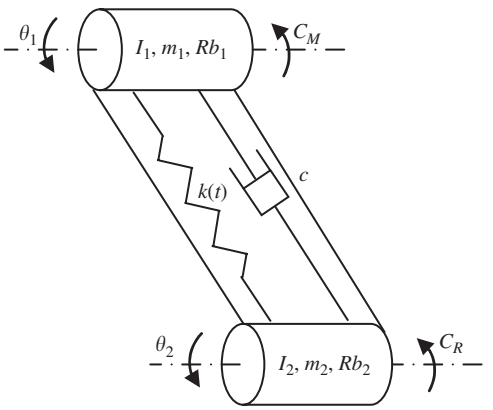

Fig. 1. Torsional gear model.

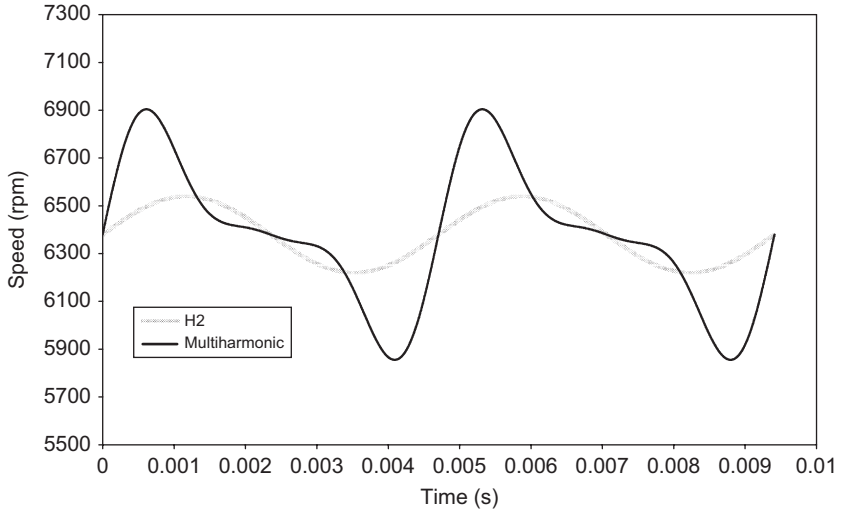

Fig. 2. Examples of engine speed fluctuations.

where Ω_{10} is the nominal average angular velocity (constant), k is the harmonic of the rotational speed, ρ_k is the corresponding dimensionless amplitude and φ_k is the initial phase. Note that the actual speeds of the pinion and the gear are $\Omega_1(t)+\dot{\theta}_1$ and $u\Omega_1(t)+\dot{\theta}_2$, respectively.

The mesh stiffness function which accounts for the tooth contact evolutions with rotation can be decomposed into a Fourier series of generic terms $\cos nZ_1\vartheta$ and $\sin nZ_1\vartheta$, where $\vartheta=\int_0^t \Omega_1(\xi)\,\mathrm{d}\xi$. As a direct consequence of the speed fluctuations in Eq. (2), the mesh stiffness spectrum comprises frequencies at $nZ_1\Omega_{10}$, the nominal meshing frequency and its harmonics, plus frequency modulations caused by the time variations in $\Omega_1(t)$. As opposed to the classical constant speed approach, the system period is one pinion revolution and not the mesh period.

The stability analysis is conducted using the homogeneous equation associated with Eq. (1):

$$\ddot{\Delta}+2\varepsilon\omega_0\dot{\Delta}+\omega_0^2(1+\alpha\phi(t))\Delta=0, \tag{3}$$

in which, $\phi(t)$ being periodic, is a Mathieu–Hill equation.

According to Floquet's theory [8], the normal form of the solution to Eq. (3) is:

$$\Delta=e^{\gamma t}G(t), \tag{4}$$

with $G(t)=G(t+T)$.

Stability is therefore controlled by the characteristic exponent γ and the solution is unstable when the real part of γ is positive.

Introducing the state vector $\mathbf{X}(t)=[{}^{\Delta(t)}_{\dot{\Delta}(t)}]$, it can be shown in Ref. [9] that there is a unique matrix $\mathbf{R}$, independent of the initial conditions, known as the monodromy matrix which relates the solutions at two successive periods by:

$$\mathbf{X}(t+nT)=\mathbf{R}\cdot\mathbf{X}(t+(n-1)T). \tag{5}$$

Stability is then characterised by the amplitudes of the eigenvalues λ_l of $\mathbf{R}$, i.e. the system is unstable when at least one of the eigenvalues is such that $|\lambda_l|>1$.

3. Stability analysis using a Newmark scheme

The literature on the dynamic stability of Mathieu–Hill equations is vast and some valuable syntheses can be found in the classic textbooks of Bolotin [9], Nayfeh and Mook [10], etc. In this paper, a numerical approach based on the time-step calculation of the monodromy matrix using an implicit Newmark scheme is applied to the particular case of gears with velocity-modulated time-varying mesh stiffness.

Following Refs. [11,12], the equation of motion (3) is discretised under the form

$$\left[\frac{4}{\mathrm{d}t^2}+\frac{4}{\mathrm{d}t}\varepsilon\omega_0+\omega_0^2(1+\alpha\phi(t+\mathrm{d}t))\right]\Delta(t+\mathrm{d}t) = \left[\ddot{\Delta}(t)+\frac{4}{\mathrm{d}t}\dot{\Delta}(t)+\frac{4}{\mathrm{d}t^2}\Delta(t)\right]+2\varepsilon\omega_0\left[\dot{\Delta}(t)+\frac{2}{\mathrm{d}t}\Delta(t)\right], \tag{6}$$

where $\mathrm{d}t$ is a constant time-step.

Substituting with the acceleration at t derived from Eq. (3) as:

$$\ddot{\Delta}(t) = -2\varepsilon\omega_0\dot{\Delta}(t)-\omega_0^2(1+\alpha\phi(t))\Delta(t), \tag{7}$$

the following form is obtained:

$$\ddot{\Delta}(t+\mathrm{d}t) = \frac{B(t+\mathrm{d}t)}{A(t+\mathrm{d}t)}\Delta(t)+\frac{D}{A(t+\mathrm{d}t)}\dot{\Delta}(t), \tag{8}$$

with

$$A(t+\mathrm{d}t) = \left[\frac{4}{\mathrm{d}t^2}+\frac{4}{\mathrm{d}t}\varepsilon\omega_0+\omega_0^2(1+\alpha\phi(t+\mathrm{d}t))\right],$$
$$B(t+\mathrm{d}t) = \left[\frac{4}{\mathrm{d}t^2}+\frac{4}{\mathrm{d}t}\varepsilon\omega_0-\omega_0^2(1+\alpha\phi(t+\mathrm{d}t))\right],$$
$$D = \frac{4}{\mathrm{d}t}.$$

The application of the Newmark scheme on speeds leads to:

$$\dot{\Delta}(t+\mathrm{d}t) = \frac{2}{\mathrm{d}t}\left(\frac{B(t+\mathrm{d}t)}{A(t+\mathrm{d}t)}-1\right)\Delta(t)+\left(\frac{2}{\mathrm{d}t}\frac{D}{A(t+\mathrm{d}t)}-1\right)\dot{\Delta}(t) \tag{9}$$

and the transition matrix which relates the state vector between two successive time-steps is derived from Eqs. (8) and (9) as:

$$\dot{\mathbf{X}}(t+\mathrm{d}t) = \mathbf{R_1}\cdot\mathbf{X}(t), \tag{10}$$

with

$$\mathbf{R}_1 = \begin{bmatrix} \dfrac{B(t+\mathrm{d}t)}{A(t+\mathrm{d}t)} & \dfrac{D}{A(t+\mathrm{d}t)} \\ \dfrac{2}{\mathrm{d}t}\left(\dfrac{B(t+\mathrm{d}t)}{A(t+\mathrm{d}t)}-1\right) & \dfrac{2}{\mathrm{d}t}\dfrac{D}{A(t+\mathrm{d}t)}-1 \end{bmatrix}.$$

The monodromy matrix is finally obtained by multiplying the transition matrices so that a complete period T of the system is covered, i.e. one complete pinion revolution in the example treated:

$$\mathbf{R} = \prod_{j=1}^{N}\mathbf{R}_j, \quad \text{with } N = \frac{T}{\mathrm{d}t} \tag{11}$$

and stability is studied by analysing the amplitudes of the eigenvalues of $\mathbf{R}$.

4. Applications

For the sake of simplicity, the applications to geared systems in this paper are confined to two idealised cases: (a) a piecewise variation which, to a certain extent, can be used for the simulations of spur gears and (b) a sinusoidal variation which is more representative of helical gear time-varying mesh stiffness (Fig. 3). The gear data are synthesised in Table 1.

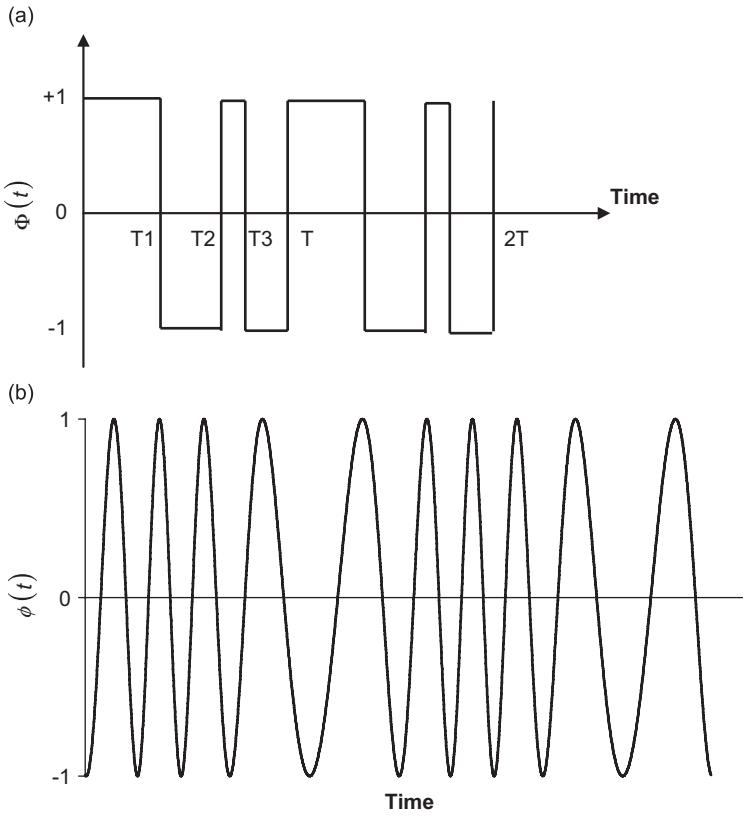

Fig. 3. Examples of modulated mesh stiffness functions: (a) piecewise constant mesh stiffness function and (b) sinusoidal mesh stiffness function.

Table 1
Gear data

	Pinion		Gear
Module (mm)	2		2
Pitch diameter (m)	0.06		0.09
Tooth number, Z_1, Z_2	30		45
Mass (kg)	1.65		3.7125
Speed ratio, u		2/3	
Damping factor, ε		0 and 0.01	
Pressure angle, α_0 (en °)		20	
Base helix angle, β_b (en °)		0, 30	

Two different time-varying engine speed models have been considered:

(i) a single H_2 harmonic variation of speed (modulation at twice the rotational speed) which is frequently employed in the literature [1],
(ii) a more realistic multi-frequency representation comprising H_2, H_4, and H_6 harmonics with relative amplitudes of 1, 0.75 and 0.25 respectively which is more representative of actual situations.

For the two cases above, 0%, 2.5%, 5%, 7.5% and 10% of speed variation (peak-to-peak) are considered. From a numerical point of view, integrations were performed (a) with 32 time-steps per mesh cycle, i.e. 960 time-steps over the system period for the sinusoidal stiffness function and (b) with $64 \times 30 = 1920$ time-steps in the case of the piecewise stiffness. Several numerical tests were conducted with finer time-steps which showed no significant variations in the stability boundaries.

It is well known that, for steady state conditions, instability occurs in the vicinity of the critical frequencies defined as [13–15]:

$$\frac{Z_1\Omega_{10}}{\omega_0} = \frac{2}{q}; \quad q = \text{integer}, \tag{12}$$

with Z_1, pinion tooth number.

In what follows, computations have been performed in the frequency ranges near the major instability zones for $q = 1$ and $q = 2$. The results obtained in the vicinity of $q = 1$ which are given in the form of 3D charts (Figs. 4–7) show the instability areas (shaded) versus frequency and mesh stiffness variations (parameter α) for various speed fluctuation amplitudes. From these stability diagrams, the following observations can be made:

(a) Regardless of the speed variation characteristics and mesh stiffness functions, the width of the unstable areas increases as the mesh stiffness variation amplitude α becomes higher.
(b) Engine speed fluctuations are found to generate additional secondary instabilities equally spaced around the main area probably caused by modulation side-bands. Compensation is observed between the main and lateral unstable zones in terms of frequency bandwidth.
(c) Instabilities are broader in the case of a piecewise constant stiffness function compared to a smoother sinusoidal time variation.
(d) Multi-harmonic engine speed fluctuations generate more instability side-bands than mono-harmonic ones because of their wide ranging spectral contents.

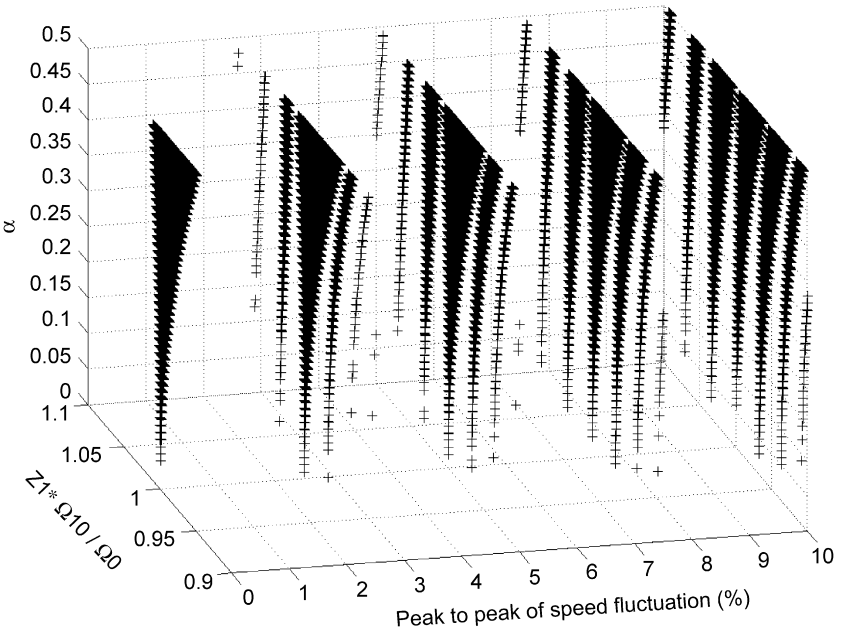

Fig. 4. Stability diagram—mono-harmonic H_2 speed fluctuation, sinusoidal mesh stiffness—no damping (*shaded areas correspond to instability*).

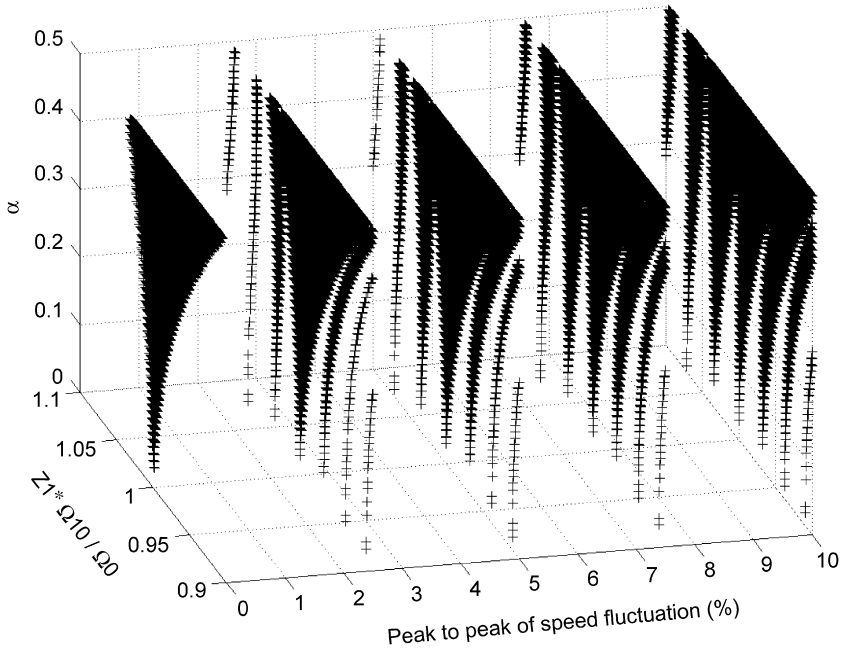

Fig. 5. Stability diagram—mono-harmonic H_2 speed fluctuation, piecewise constant mesh stiffness—no damping (*shaded areas correspond to instability*).

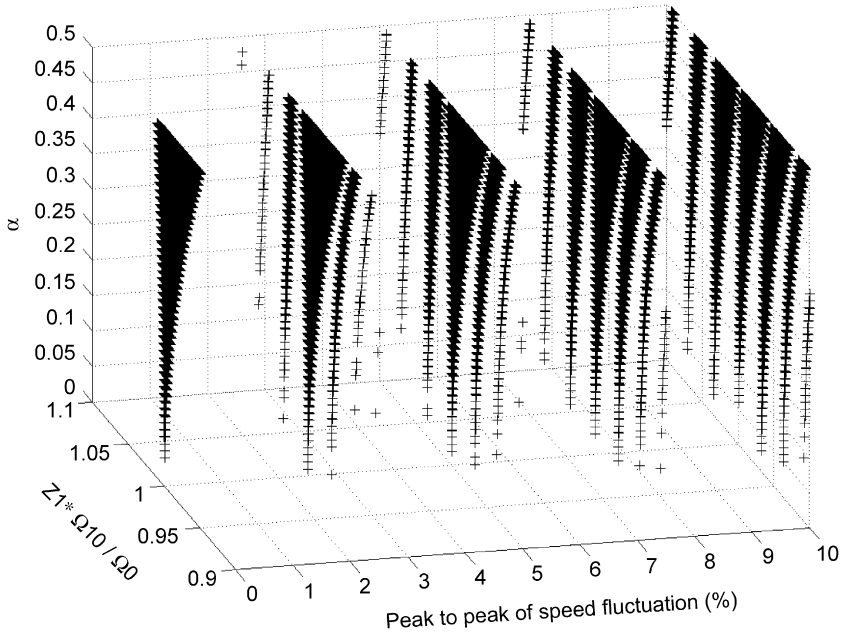

Fig. 6. Stability diagram—multi-harmonic speed fluctuation, sinusoidal mesh stiffness—no damping (*shaded areas correspond to instability*).

From the analytical analysis of the dynamic response presented in Ref. [16], the potentially critical frequencies for tooth loading were found to be:

$$\frac{Z_1\Omega_{10}}{\omega_0} = \frac{2}{q(1 \pm (hk/Z_1))}, \quad h = 2k,\ 2k \pm 1,\ 2k - 2, \tag{13}$$

which correspond to the instability areas observed in Figs. 4–7.

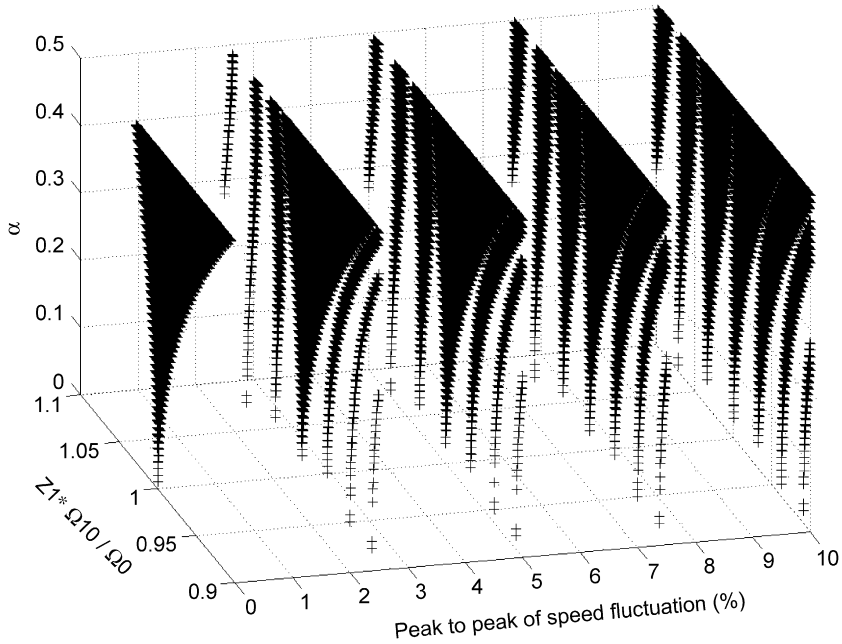

Fig. 7. Stability diagram—multi-harmonic speed fluctuation, piecewise constant mesh stiffness—no damping (*shaded areas correspond to instability*).

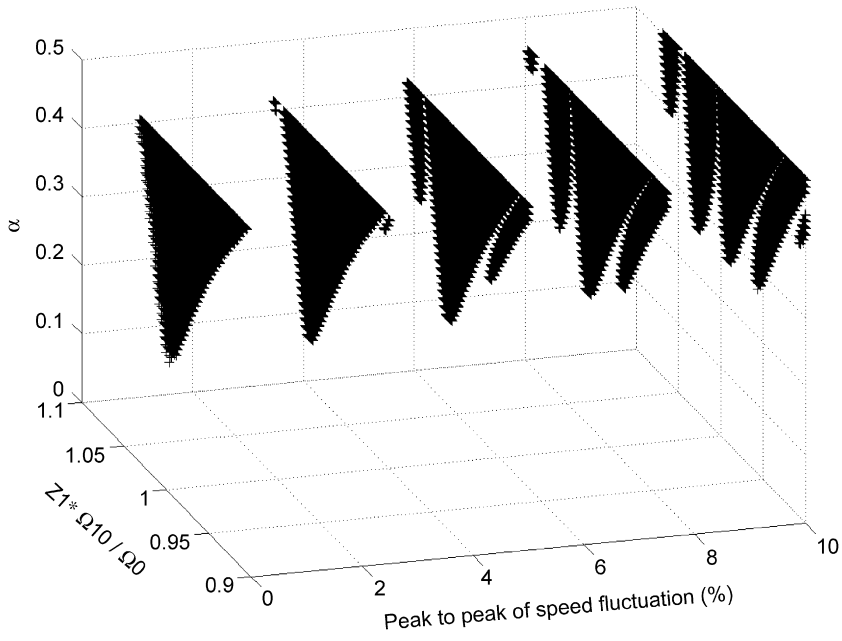

Fig. 8. Stability diagram—mono-harmonic H_2 speed fluctuation, piecewise constant mesh stiffness—damping factor of 0.01 (*shaded areas correspond to instability*).

The influence of damping is illustrated in Figs. 8 and 9 which show the stability charts obtained with a damping ratio of 0.01. As expected, damping pushes instabilities towards the higher values of α and reduces the number of unstable zones related to side-bands. Here again, a piecewise constant mesh stiffness function (representative of spur gears, say) is more detrimental than a sinusoidal variation.

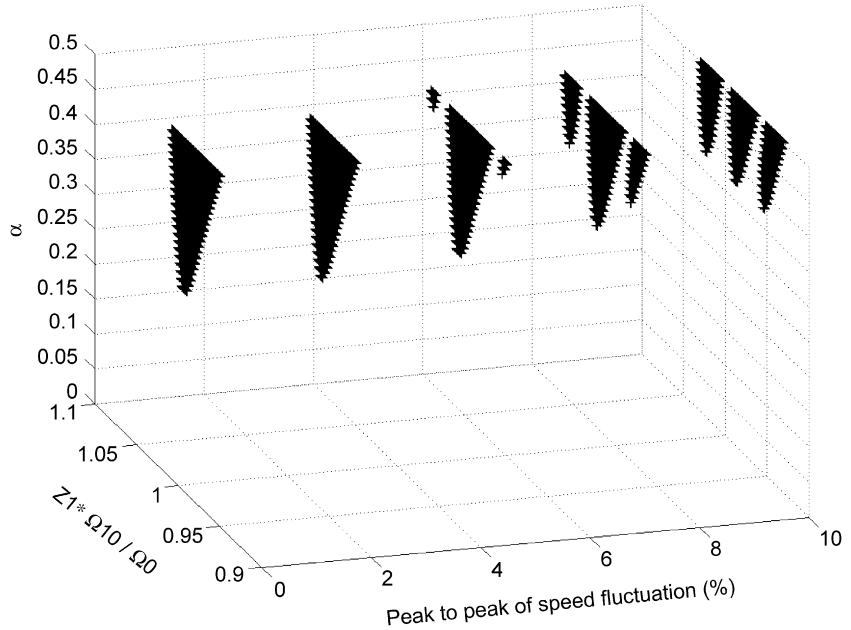

Fig. 9. Stability diagram—mono-harmonic H_2 speed fluctuation, sinusoidal mesh stiffness—damping factor of 0.01 (*shaded areas correspond to instability*).

Similar trends have been found near $q = 2$ however, because of space limitations, they are not reported in this paper.

5. Conclusion

An original model has been presented which accounts for periodic speed fluctuations in geared systems. The corresponding parametrically excited differential equation exhibits frequency modulated time-varying mesh stiffness functions which depend on gear geometry and on the characteristics of engine speed variations. Based on a Newmark scheme, a time-step numerical technique is presented for calculating the monodromy matrix and analysing the system instability. Several stability diagrams are shown which illustrate the roles of the mesh stiffness variation amplitude and shape, the characteristics of speed fluctuations and damping. It is found that additional unstable areas are generated around the major instability typical of gears at constant speed and that the bandwidths of all the unstable zones are interdependent. Further research is under way in order to generalise this approach to three-dimensional models and more realistic gear geometries with tooth modifications and errors.

References

[1] J.L. Ligier, E. Baron, Acyclisme et vibrations, Applications aux moteurs thermiques et aux transmissions, Publications de l'Institut Français de Pétrole et de Moteurs, Editions TECHNIP, Paris, Vol. 1, 2002, 102pp.
[2] Ph. Couderc, J. Callenaere, J. Der Hagopian, G. Ferraris, A. Kassai, Y. Borjesson, L. Verdillon, S. Gaimard, Vehicle driveline dynamic behaviour: experimentation and simulation, *Journal of Sound and Vibration* 218 (1) (1998) 133–157.
[3] M. Barthod, B. Hayne, J.L. Tébec, J.C. Pin, Experimental study of dynamic and noise produced by a gearing excited by a multi-harmonic excitation, *Applied Acoustics* 68 (9) (2007) 1003–1025.
[4] S.L. Harris, Dynamic loads on the teeth of spur gears, *Proceedings of the Institution of Mechanical Engineers* 172 (1958) 87–112.
[5] R.W. Gregory, S.L. Harris, R.G. Munro, Dynamic behaviour of spur gears, *Proceedings of the Institution of Mechanical Engineers* 178 (1963) 261–266.
[6] H.N. Ozgüven, D.R. Houser, Mathematical models used in gear dynamics—a review, *Journal of Sound and Vibration* 121 (1988) 383–411.

[7] J. Wang, R. Li, X. Peng, Survey of non-linear vibration of gear transmission systems, *Applied Mechanics Reviews* 56 (3) (2003) 309–329.
[8] M.G. Floquet, Sur les équations différentielles linéaires à coefficients périodiques, Février, Annales de l'Ecole Normale, 2ème série, Tome XII (1883) 47–89.
[9] V.V. Bolotin, *The Dynamic Stability of Elastic Systems*, Holden-Day, San Francisco, 1964, pp. 145–277.
[10] A.H. Nayfeh, D.T. Mook, *Non Linear Oscillations*, Wiley, New York, 1979, pp. 258–365.
[11] P.M. Guilhen, P. Berthier, G. Ferraris, M. Lalanne, Dynamic behavior of dissymmetric rotor bearings modelled with a periodic coefficient large system, in: The 58th Shock and Vibration Symposium, Vol. 1, NASA-Marshall Space Flight Center, 1987, pp. 487–494.
[12] P. Velex, Contribution à l'Analyse du Comportement Dynamique de Réducteurs à Engrenages à Axes Parallèles, Ph.D. Dissertation, INSA de Lyon, 1988, No. 88, ISAL 0032, 188pp.
[13] M. Benton, A. Seireg, Simulation of resonances and instability conditions in piniongeared systems, *ASME, Journal of Mechanical Design* 100 (1978) 26–32.
[14] M. Benton, A. Seireg, Factors influencing instability and resonance in geared systems, *ASME, Journal of Mechanical Design* 103 (1981) 372–378.
[15] M. Amabili, A. Rivola, Dynamic analysis of spur gear pairs: steady-state response and stability of the SDOF model with time-varying mesh damping, *Mechanical Systems and Signal Processing* 11 (1997) 375–390.
[16] G. Sika, P. Velex, Analytical and numerical dynamic analysis of gears in the presence of engine acyclism, *Proceedings of the ASME 2007 International Design Engineering Technical Conferences and Computers and Information in Engineering Conference*, September 4–7, 2007, Las Vegas, Paper DETC2007-34068.